Microscopy and Microanalysis, 2026, **32**, ozag016
https://doi.org/10.1093/mam/ozag016
Advance access publication 18 March 2026
Original Article

Microscopy AND Microanalysis

Label-Free Imaging of Red Blood Cells in Gestational Diabetes: Autofluorescence Captures Oxidative Stress Beyond Membrane Fluidity

Alessia Riente[1,2,†], Caterina Neri[3,†], Duaa Hatem[1,2], Cassandra Serantoni[1,2], Michele Maria De Giulio[1,2], Davide Archelao Dessì[3], Davide Manieri[3], Alessandro Rizzi[4], Linda Tartaglione[4], Lorenzo Lucacchini Paoli[4], Marco De Spirito[1,2], Giuseppe Maulucci[1,2,*,‡], and Dario Pitocco[4,‡]

[1]*Metabolic Intelligence Lab, Department of Neuroscience, Università Cattolica del Sacro Cuore, Largo Francesco Vito, 1, Rome, 00168, Italy*
[2]*UOC Physics for Life Sciences, Fondazione Policlinico Universitario "A. Gemelli" IRCCS, Largo Agostino Gemelli, 8, Rome, 00168, Italy*
[3]*Department of Women and Child Health, Women Health Area, Fondazione Policlinico Universitario "A. Gemelli" IRCCS, Largo Agostino Gemelli, 8, Rome, 00168, Italy*
[4]*Diabetes Care Unit, Fondazione Policlinico "A. Gemelli" IRCCS - Università Cattolica del Sacro Cuore, Largo Agostino Gemelli, 8, Rome, 00168, Italy*

*__Corresponding author__. Giuseppe Maulucci, E-mail: giuseppe.maulucci@unicatt.it

[†]The authors contributed equally to this work.

[‡]Senior Authors.

Abstract

Gestational diabetes mellitus (GDM) is a transient pregnancy disorder marked by insulin resistance and oxidative stress. In type 1 and 2 diabetes, reduced red blood cell (RBC) membrane fluidity, measured by Laurdan-GP, associates with vascular risk, but its role in GDM is unclear. This study compared GP with intrinsic RBC autofluorescence (green-to-red ratio, $AF_{G,R}$) to identify a better marker of metabolic stress in GDM. Forty-eight pregnant women were enrolled (31 GDM, 17 controls). High-resolution multispectral confocal imaging quantified RBC GP and $AF_{G,R}$. A machine-learning pipeline analyzed core, membrane, and whole-cell metrics, alongside clinical and biochemical data. Logistic regression assessed associations with GDM. GP did not differ between groups (0.60 ± 0.04 versus 0.61 ± 0.04; $p = 0.168$), unlike the reductions reported in chronic diabetes. Conversely, $AF_{G,R}$ values were higher in GDM across compartments (core: -0.073 ± 0.202 versus -0.154 ± 0.060; membrane: 0.013 ± 0.198 versus -0.066 ± 0.075; $p = 0.049$). In multivariable analysis, $AF_{G,R}$ Core independently predicted GDM status ($p = 0.018$), outperforming clinical and hematological markers. In GDM, membrane fluidity remains unchanged, but RBC autofluorescence reflects acute oxidative stress, supporting its use as a non-invasive, repeatable complement to OGTT for early risk assessment and monitoring.

Key words: autofluorescence imaging, gestational diabetes mellitus, metabolic biomarkers, oxidative stress, red blood cells

Received: October 13, 2025. **Revised:** February 11, 2026. **Accepted:** February 24, 2026

Graphical Abstract

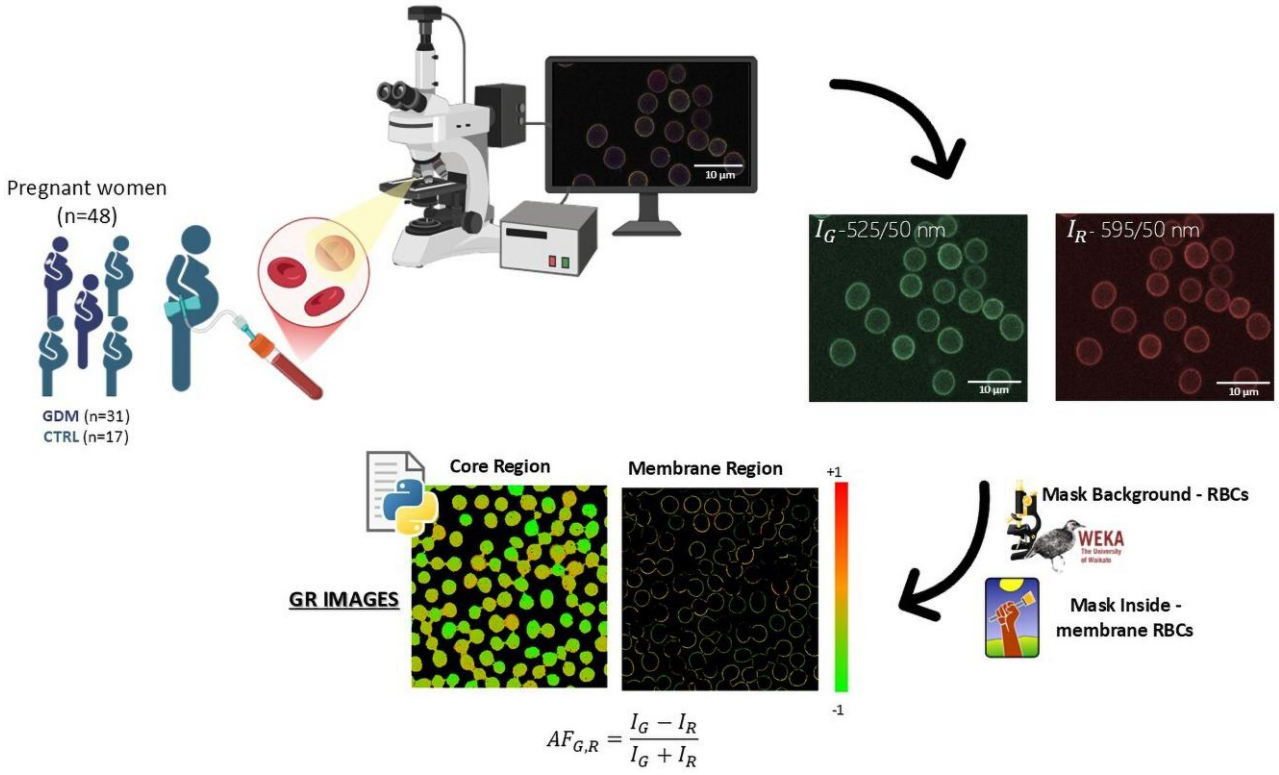

Abbreviations: AF, autofluorescence; ALT, alanine aminotransferase; AST, aspartate aminotransferase; BMI, body mass index; CTRL, control; DMSO, dimethyl sulfoxide; FAD, Flavin adenine dinucleotide; FDR, false discovery rate; FLIM, fluorescence lifetime imaging microscopy; GaAsP, gallium arsenide phosphide; GDM, gestational diabetes mellitus; GP, generalized polarization; Hb, hemoglobin; HDL/LDL, high-/low-density lipoprotein ratio; IR, insulin resistance; NADH/NAD(P)H, nicotinamide adenine dinucleotide (reduced)/nicotinamide adenine dinucleotide (phosphate); OGTT, oral glucose tolerance Test; OR, odds ratio; RBC(s), red blood cell(s); T1DM/T2DM, type 1/type 2 diabetes mellitus; WBC, white blood cell count.

Introduction

Gestational diabetes mellitus (GDM) is a metabolic disorder characterized by glucose intolerance with onset or first recognition during pregnancy (American Diabetes Association Professional Practice Committee, 2024). It affects approximately 7–14% of pregnancies worldwide and is associated with both short- and long-term complications for the mother and offspring, including increased risk of type 2 diabetes, preeclampsia, macrosomia, and metabolic syndrome (Chiefari et al., 2017; McIntyre et al., 2019). GDM is marked by insulin resistance, systemic inflammation, and oxidative stress, all of which can impact cellular and subcellular homeostasis, including red blood cell (RBC) physiology (Saucedo et al., 2023). Membrane fluidity is a fundamental biophysical property of biological membranes, playing a pivotal role in a wide range of cellular functions, including molecular transport, signal transduction, and mechanical adaptability. In RBCs, membrane fluidity is especially critical for preserving cell deformability and ensuring effective microcirculatory flow (Pitocco et al., 2025). This property is modulated by several interdependent factors, such as lipid composition, temperature, protein–lipid interactions, and post-translational modifications, including glycation and oxidation (Maulucci et al., 2017; Pitocco et al., 2025). These mechanisms are particularly relevant in pathological conditions like DM, where systemic metabolic alterations, including oxidative stress and lipid imbalance, deeply impact the structural and functional integrity of the RBC membrane (Lyons & Basu, 2012; Rajab et al., 2018; Li et al., 2023). In patients with diabetes, RBC membrane fluidity is often increased due to enhanced glycation, oxidative damage, and altered lipid distribution (Bianchetti et al., 2024; Pitocco et al., 2025). These biophysical changes have been associated with impaired erythrocyte function and the development of both microvascular and macrovascular complications, such as diabetic retinopathy and peripheral artery disease (Bianchetti et al., 2021, 2022; Ebenuwa et al., 2024). A well-established method to assess membrane fluidity is Laurdan-based generalized polarization (GP) imaging, which is highly sensitive to lipid packing and membrane hydration states (Maulucci et al., 2017; Bianchetti et al., 2019). Laurdan fluorescence has been successfully employed to detect submicrometric changes in membrane phase behavior in RBCs from diabetic patients (Bianchetti et al., 2024). Cross-sectional evidence from type 1 and type 2 diabetes indicates that long-standing metabolic stress can lead to stable lipid remodeling of the RBC membrane, detectable as reduced fluidity and associated with vascular complications (Bianchetti et al., 2021, 2024; Ebenuwa et al., 2024). However, GDM differs from chronic diabetes in both duration and pathophysiology: being a transient condition, it may not provide sufficient time for persistent lipid-phase alterations to

emerge. In this scenario, it is reasonable to investigate whether GDM, although distinct in pathophysiology and timescale from T1DM and T2DM, also induces detectable changes in RBC membrane fluidity. At the same time, current screening for GDM relies exclusively on glucose handling (e.g., OGTT), and may overlook early oxidative or metabolic stress. Therefore, more dynamic indicators may be required: in particular, RBC intrinsic autofluorescence (AF) is highly sensitive to acute redox imbalance, potentially capturing metabolic stress in GDM that fluidity fails to detect. AF originates from endogenous fluorophores such as flavins (e.g., FAD), NAD(P)H, and porphyrins (Fauaz et al., 2010; Croce & Bottiroli, 2014; Shrirao et al., 2021). In particular, the green-to-red autofluorescence ratio ($AF_{G,R}$) integrates changes in flavin and porphyrin signals, positioning it as a sensitive indicator of oxidative stress and metabolic remodeling. AF originates from intrinsic fluorophores such as flavins (e.g., flavin adenine dinucleotide, FAD), nicotinamide adenine dinucleotide (NADH), porphyrins (e.g., protoporphyrin IX), and lipofuscin-like compounds (Fauaz et al., 2010; Croce & Bottiroli, 2014; Shrirao et al., 2021). These molecules are involved in key metabolic and oxidative processes, making AF a sensitive, label-free indicator of cellular function and stress. Therefore, in this study, two approaches in parallel have been tested: Laurdan-based GP to probe RBC membrane fluidity, and $AF_{G,R}$ to assess metabolic alterations. This dual strategy was designed to capture potential biophysical and metabolic signatures of GDM, and to evaluate their relative discriminative value compared with standard clinical parameters.

Materials and Methods

Prospective single-center observational study (Rome, September 2020–June 2024) comparing GDM and controls on RBC Laurdan-GP and autofluorescence; reporting adheres to STROBE (checklist in Supplementary Information).

Study Participants and Data Preprocessing

A total of 48 women with singleton pregnancy, including 17 healthy controls and 31 women with gestational diabetes mellitus (GDM), were enrolled at the Diabetes Care Unit of Fondazione Policlinico Universitario "A. Gemelli" IRCCS (Rome, Italy) between September 2020 and June 2024. In this prospective observational study, the cohort had a mean age of 33.7 years (±4.1), with an average pre-pregnancy weight of 64.7 kg (±14.9) and a BMI of 23.9 kg/m^2 (±5.5). The mean gestational weight gain was 7.8 kg (±4.3). Participants reported an average of 2.2 pregnancies (±1.1), with a mean parity of 0.67 (±0.79), indicating that many were in their first ongoing pregnancy. Most individuals were of Caucasian ethnicity (89.4%), followed by Hispanic (6.4%) and Asian (4.3%) backgrounds. Also, 10.6% were smokers during pregnancy (regardless of the trimester), while 89.4% were either non-smokers or had quit before pregnancy onset. GDM was diagnosed with the standard screening at 24–28 weeks of gestation with a 75 gr glucose tolerance test. Participants were eligible if they had a singleton pregnancy, were older than 18 years, were able to provide written informed consent, and, in the case of the GDM group, received a diagnosis at 24–28 weeks of pregnancy. Exclusion criteria included multiple pregnancy, maternal age under 18 years, pre-existing type 1 or type 2 diabetes mellitus, autoimmune or hematological diseases, and inability to sign or comprehend informed consent.

The dataset analyzed in this study was derived from a broader clinical and laboratory database initially. Prior to statistical analysis, a comprehensive data cleaning and variable selection process was performed. Variables were excluded based on predefined criteria, including redundancy (e.g., overlapping or highly correlated measures), lack of variability, or insufficient data availability. Following this filtering step, 28 descriptive features were retained, encompassing RBC autofluorescence parameters and GP as well as selected anthropometric, clinical, biochemical, and obstetric variables. Where data were missing, analyses relied on the available observations; variables affected are indicated.

The retained variables were grouped into four categories:

- *Anthropometric, demographic, and lifestyle characteristics*: maternal age, pre-pregnancy weight, BMI, and gestational weight gain; obstetric history (gravidity and parity); ethnicity (Asian, Caucasian, Hispanic); and smoking status (non-smokers/former smokers versus current smokers).
- *Pregnancy-related parameters and neonatal outcomes*: gestational age at testing and delivery; delivery mode (spontaneous vaginal, operative vaginal, cesarean section); neonatal sex; and Apgar score at 1 min postpartum.
- *Clinical and biochemical parameters*: fasting glucose, 60- and 120-min OGTT glucose values, serum triglycerides, HDL/LDL ratio, uric acid, creatinine, liver enzymes (ALT, AST), hematological parameters (WBC, Hb, MCV), and mean arterial pressure.
- *Autofluorescence parameters and GP values*: RBC autofluorescence quantified as $AF_{G,R}$ in the cell core, membrane, and whole-cell areas. In addition, membrane fluidity was assessed through Laurdan-based GP, providing a measure of lipid packing and order. Both procedures are described in Section "Image Analysis".

This research was approved by the ethics committee, and all clinical investigations were conducted in accordance with the principles of the Declaration of Helsinki. Written informed consent was obtained from all participants prior to enrollment.

Sample Preparation and Fluidity Measurement of RBCs' Membrane

Blood samples, collected in heparinized tubes, were suspended in physiological saline solution (0.9% NaCl) at a 1:1,000 dilution, seeded in multi-well plates (ibidi, GmbH), and immediately processed for imaging. For membrane fluidity analysis, erythrocytes were additionally labeled with Laurdan (1 μM), as previously reported. All measurements were performed using a Nikon A1-MP inverted confocal microscope equipped with a 60× oil-immersion objective (NA = 1.4) and an on-stage incubator (37° C, 5% CO_2, OKOLAB). For autofluorescence, emission was simultaneously collected in three spectral channels (450/50 nm, 525/50 nm, 595/50 nm). For membrane fluidity, Laurdan was excited at 402 nm and emission was recorded at 450/50 nm and 525/50 nm to calculate GP values. Images were acquired with a GaAsP detector at 16-bit depth, 0.25 ms dwell time, and line averaging (×2). Optical magnification was set at 2.89×, with a resolution of 1,024 × 1,024

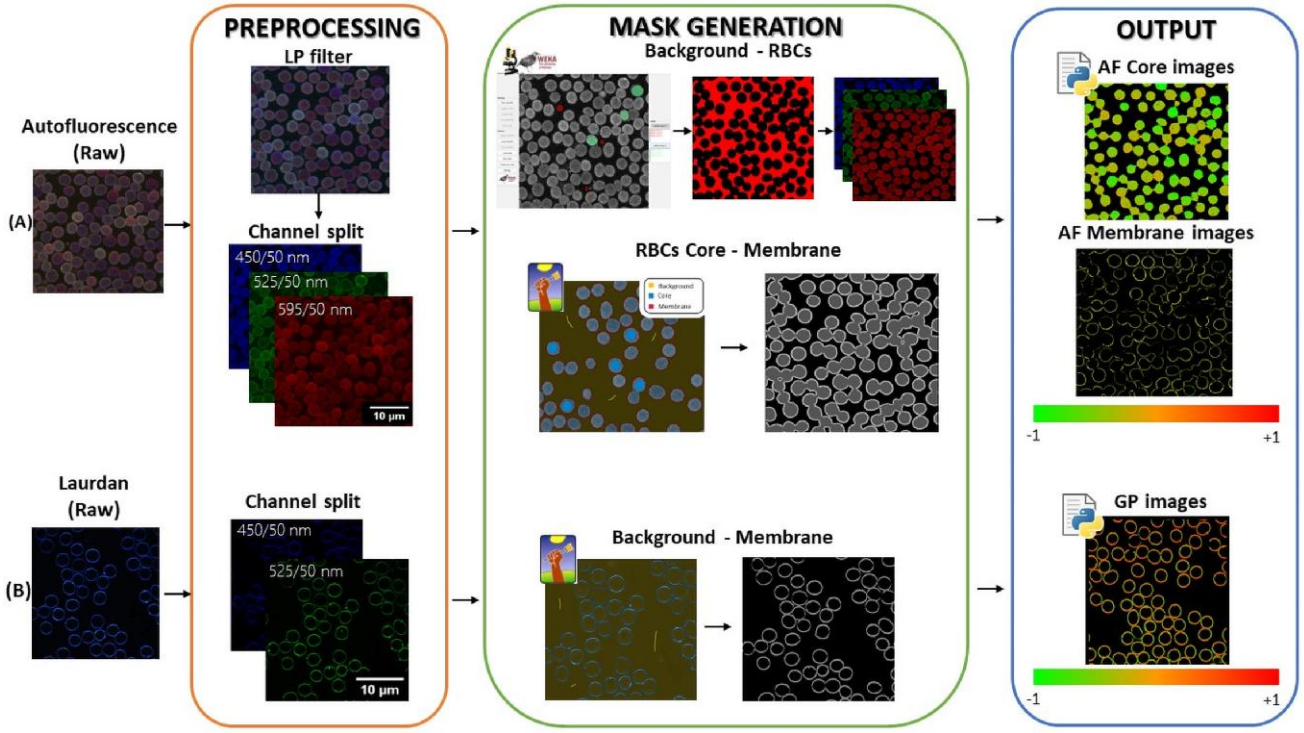

Fig. 1. Analytical workflow for label-free RBC imaging. (**a**) Processing pipeline for autofluorescence imaging: raw multispectral stacks were preprocessed and separated into three spectral channels (450/50 nm, 525/50 nm, and 595/50 nm), followed by machine-learning-based segmentation (WEKA, Ilastik) to identify background, membrane, and core compartments. Ratios between 525/50 nm and 595/50 nm channels were computed per pixel to obtain compartment-specific autofluorescence maps. (**b**) The Laurdan-based GP workflow: Laurdan-labeled cells were excited at 402 nm and emission collected at 450/50 nm and 525/50 nm; GP values were calculated at the membrane level using a calibration factor. Final outputs are pseudocolored maps ranging from −1 to +1.

pixels. For each sample, at least three images were collected (~150 erythrocytes).

Image Analysis

To perform a quantitative analysis of RBC AF ratio, a multistep image processing pipeline was developed. Initially, raw image stacks were subjected to low-pass filtering to suppress high-frequency noise and enhance signal homogeneity across the field of view. Subsequently, the filtered images were split into three separate spectral channels, corresponding to emission wavelengths of 450/50 nm (blue), 525/50 nm (green), and 595/50 nm (red), to isolate distinct AF components associated with different fluorophores. To differentiate RBCs from the background, a supervised pixel classification approach was employed using the WEKA Trainable Segmentation plugin integrated in FIJI/ImageJ. This step generated binary masks identifying RBC regions, which were then applied to the channel-separated images to exclude non-cellular areas. For finer structural delineation, particularly to distinguish the core space from the cell membrane, an additional classification step was carried out using Ilastik, an interactive machine learning-based image analysis platform. This allowed for the generation of a three-class probability mask segmenting each image into background, core, and membrane regions. Morphological refinement was applied to improve membrane continuity and accuracy. These masks were subsequently overlaid onto the original fluorescence images to extract pixel-wise intensity values for the green and red channels within each defined region of interest. An $AF_{G,R}$ ratio index was then computed on a per-pixel basis using the formula:

$$AF_{G,R} = \frac{I_G - I_R}{I_G + I_R} \quad (1)$$

Where I_G and I_R represent the intensity values from the green and red channels, respectively. Separate GR ratio maps were generated for both the core and membrane compartments of each RBC, enabling spatially resolved analysis of AF patterns and supporting quantitative comparisons across samples.

For the analysis of membrane fluidity, Laurdan-based generalized polarization (GP) imaging was performed. Blue (I_B, 450/50 nm) and green (I_G, 525/50 nm) channels were extracted, and a binary mask of the membrane region was generated in Ilastik to exclude background and non-relevant elements. GP values were then calculated pixel-wise as:

$$GP = \frac{I_B - G \times I_G}{I_B + G \times I_G} \quad (2)$$

where I_B and I_G correspond to the blue and green Laurdan emission intensities, and G is a calibration factor obtained from Laurdan solutions in DMSO (variation <2% across the imaging area). The detailed segmentation pipeline is illustrated in Figure 1.

Statistical Analyses

All statistical analyses were performed using Python (version ≥3.8), leveraging standard libraries for data manipulation

and modeling. A comprehensive comparison was conducted between the control (CTRL) and gestational diabetes mellitus (GDM) groups. Continuous variables were analyzed using either the independent samples t-test ("*ttest_ind*" from "*scipy.stats*") or the Mann–Whitney *U* test ("*mannwhitneyu*" from "*scipy.stats*"), depending on the distribution of the data as assessed by the Shapiro–Wilk test ("*shapiro*" from "*scipy.stats*"). Categorical variables were assessed using the chi-square (χ^2) test ("*chi2_contingency*" from "*scipy.stats*"). Statistical significance was set at $p < 0.05$. To account for multiple comparisons and control the false discovery rate, *p*-values were adjusted using the Benjamini–Hochberg (FDR) correction method via the "*multipletests*" function from "*statsmodels.stats.multitest*". To further investigate the association between predictors and group membership (GDM versus CTRL), a binary logistic regression analysis was performed using the "*Logit*" function from *statsmodels*. Continuous predictors were standardized using *StandardScaler* from sklearn.preprocessing to ensure equal contribution to model estimation. As a first step, pairwise correlations among predictors were examined using the "*.corr()*" method from "*pandas*" to identify and remove highly correlated variables. Subsequently, multicollinearity was assessed by calculating the Variance Inflation Factor (VIF) with the "*variance_inflation_factor*" function from "*statsmodels.stats.outliers_influence*", applying a conservative exclusion threshold of VIF ≥ 5. Due to the sample size ($n = 48$), and in order to avoid overfitting, it was necessary to limit the number of predictors included in the multivariable model. Although all variables showed acceptable multicollinearity levels (VIF < 5) and no strong pairwise correlations, a preliminary variable selection was performed. To this end, univariate logistic regression analyses were conducted for each predictor using "*Logit*" from "*statsmodels*", to explore their individual association with group membership. To guide variable selection, predictors with a *p*-value < 0.5 in the univariate models were retained for multivariable analysis. This threshold was chosen to allow for the inclusion of potentially relevant predictors in an exploratory framework, while accounting for the limited sample size and minimizing the risk of overfitting. Based on this approach, the final model included BMI, age, MCV, and $AF_{G,R}$ Core.

Results

Characteristics of the Study Population

As shown in Table 1, several anthropometric and metabolic parameters differed between CTRL and GDM groups. Women with GDM had higher pre-pregnancy BMI and weight compared to controls (25.45 versus 21.34 kg/m^2 and 68.6 versus 58.2 kg, respectively; FDR-adjusted $p = 0.063$ for both, borderline significance). Glucose concentrations during the oral glucose tolerance test were markedly elevated in the GDM group, particularly at 60 and 120 min ($p = 0.003$ for both), while fasting glucose showed only a borderline increase ($p = 0.055$). Gestational age at delivery was slightly shorter in GDM pregnancies (38.5 versus 39.5 weeks, $p = 0.051$). Trends toward higher triglycerides and uric acid were observed in the GDM group, although these differences did not reach conventional significance thresholds ($p = 0.082$ and $p = 0.010$, respectively). In contrast, no meaningful differences were found in hematological indices (Hb, WBC, MCV), liver enzymes (AST, ALT), or mean arterial pressure. Neonatal outcomes, including sex distribution and Apgar score, were comparable between groups. Also, RBC membrane fluidity, measured by GP, did not differ significantly between groups (mean GP 0.61 versus 0.60; $p = 0.168$). Neonatal outcomes, including sex distribution and Apgar score, were comparable between groups. These findings confirm the expected metabolic impairment in GDM, characterized by increased adiposity and impaired glucose handling, while highlighting that conventional hematological parameters remain largely unaffected. This underscores the potential added value of RBC autofluorescence as a sensitive biomarker of biophysical alterations beyond standard clinical measures.

RBC Membrane Fluidity Mapping

To investigate whether gestational diabetes mellitus affects RBC membrane fluidity, Laurdan-based GP imaging was performed. Representative GP maps are shown in Figure 2, panels A–B, with corresponding quantitative analysis in panel C. In contrast to previous findings in type 1 and type 2 diabetes—where significant alterations in GP values have been documented (Bianchetti et al., 2021, 2024) RBCs from GDM patients did not exhibit measurable differences in membrane fluidity compared with controls. Quantitative analysis of GP values at the membrane level confirmed this observation: the mean GP was comparable between CTRL and GDM groups (CTRL: 0.61 ± 0.04; GDM: 0.60 ± 0.04; $p = 0.168$), with overlapping distributions across all samples (Fig. 2, panel C). No significant changes were observed either in this compartmentalized analysis. These results indicate that, on the timescale and metabolic context of gestational diabetes, RBC membrane fluidity remains unaltered. This contrasts with the marked GP alterations observed in chronic diabetes (T1DM, T2DM) and suggests that GP is not a sensitive biomarker of metabolic stress in GDM. Consequently, alternative approaches such as autofluorescence analysis may provide more informative readouts of disease-related alterations.

Red Blood Cell Autofluorescence Mapping

Figure 3 shows representative $AF_{G,R}$ maps and their quantitative analysis. CTRL RBCs (A, C) exhibit $AF_{G,R}$ values predominantly in the negative range (green–yellow scale), whereas GDM RBCs (B, D) shift toward higher, positive values (orange–red). Panel E quantifies these differences: both the core and membrane compartments present a significant upward shift in GDM compared with CTRL (core: -0.073 ± 0.202 versus -0.154 ± 0.060; membrane: 0.013 ± 0.198 versus -0.066 ± 0.075; both $p = 0.049$). When considering the entire RBC area, a global increase in $AF_{G,R}$ persisted in GDM (-0.058 ± 0.199 versus -0.135 ± 0.055; $p = 0.049$). These results indicate that GDM RBCs are characterized by a reproducible shift toward higher $AF_{G,R}$ values across all compartments. Statistical comparisons are summarized in Table 1, together with other clinical and biochemical parameters.

Effect of BMI on RBC Autofluorescence in Non-GDM Controls

To evaluate whether metabolic status, and specifically body mass index (BMI), may influence red blood cell (RBC) autofluorescence independently of gestational diabetes, an additional analysis was performed in an independent cohort of non-GDM pregnant women ($n = 23$) characterized by a broader BMI range. This supplementary cohort included

Table 1. Clinical, Metabolic, and RBC Autofluorescence Parameters in CTRL and GDM Groups.

Features	Mean CTRL (SD) [IC 95%]	Mean GDM (SD) [IC 95%]	Median CTRL (Q1–Q3) [IC 95%]	Median GDM (Q1–Q3) [IC 95%]	% CTRL	% GDM	Stat	*p* Value
Age	33 (3.97) [30.96–35.04]	34.13 (4.13) [32.61–35.64]					−0.929	0.395
BMI*			21.08 (19.36–22.15) [18.53–26.58]	23.65 (20.65–30.13) [18.79–37.84]			141	**0.063**
Prepregnancy weight*			56.00 (54.00–62.00) [48.00–70.00]	66.00 (57.50–78.00) [49.40–98.20]			148	**0.063**
Weight delta*	8.94 (2.30) [7.76–10.13]	7.16 (5.05) [5.20–9.12]					1.609	0.172
Week Pregnancy*	29.75 (3.28) [28.00–31.50]	28.00 (3.71) [26.03–29.97]					1.415	0.230
EG at delivery (weeks)*	39.53 (1.06) [38.95–40.12]	28.00 (3.71) [26.03–29.97]					2.767	**0.051**
Base blood glucose*	77.31 (8.87) [72.59–82.04]	84.77 (10.22) [80.64–88.90]					−2.495	**0.055**
Blood glucose 60min*			135.00 (104.50–149.00) [75.70–160.60]	184.00 (144.50–195.50) [121.60–210.40]			59.5	**0.003**
Blood glucose 120min*	105.31 (21.72) [93.74–116.88]	137.72 (29.76) [125.44–150.00]					−4.023	**0.003**
Uric acid*			3.70 (3.40–3.92) [2.40–5.10]	4.50 (3.40–5.30) [2.96–6.86]			149	**0.010**
Triglycerides*	159.57 (47.74) [132.00–187.14]	218.67 (90.36) [168.63–268.71]					−2.222	**0.082**
HDL/LDL*			0.53 (0.44–0.70) [0.38–1.24]	0.49 (0.45–0.76) [0.27–0.81]			103.5	0.965
MCV*			87.20 (84.35–89.05) [75.15–91.50]	84.40 (82.65–90.00) [72.73–94.90]			282	0.392
ALT*			12.00 (11.00–14.00) [8.00–19.80]	14.00 (11.25–23.75) [7.45–49.85]			184	0.172
WBC*			9.99 (7.59–11.17) [7.32–14.86]	10.65 (9.02–13.15) [7.78–17.08]			170.5	0.172
Hb*	11.45 (1.18) [10.84–12.05]	10.99 (1.24) [10.53–11.45]					1.251	0.284
AST*			18.00 (17.00–20.00) [14.00–25.60]	16.50 (14.00–20.00) [11.00–37.75]			231.5	0.392
Mean arterial pressure*	82.78 (7.46) [78.95–86.62]	84.62 (5.17) [82.57–86.66]					−0.888	0.401
$AF_{G.R}$ Core			−0.16 (−0.19 to −0.13) [−0.22 to −0.07]	−0.11 (−0.15 to −0.06) [−0.21–0.02]			146.5	**0.051**
$AF_{G.R}$ Membrane			−0.07 (0.11 to −0.06) [−0.14–0.06]	0.03 (−0.06–0.03) [−0.13–0.19]			149	**0.051**
$AF_{G.R}$ RBCs			−0.14 (−0.17 to −0.11) [−0.20–−0.06]	−0.09 8–0.13—0.04) [−0.19–0.02]			143	**0.051**
GP*	0.62 (0.03) [0.60–0.64]	0.60 (0.04) [0.59–0.62]					1.738	0.168
Gravidity*					1.0:35% | 2.0:41% | 3.0:18% | 4.0:0.0% | 5.0:6% |	1.0:23% | 2.0:36% | 3.0:19% | 4.0:13% | 5.0:3% |	3.042	0.845

(*continued*)

Table 1. Continued

Features	Mean CTRL (SD) [IC 95%]	Mean GDM (SD) [IC 95%]	Median CTRL (Q1–Q3) [IC 95%]	Median GDM (Q1–Q3) [IC 95%]	% CTRL	% GDM	Stat	*p* Value
Parity*					0.0:47% | 1.0:41% | 2.0:6% | 4.0:6% |	0.0:42% | 1.0:45% | 2.0:7% | 4.0:0% |	1.853	0.845
Ethnicity*					0.0:6% | 1.0:82% | 2.0:12% |	0.0:3% | 1.0:90% | 2.0:3% |	1.521	0.845
Smoking*					0.0:94% | 1.0:6% |	0.0:84% | 1.0:13% |	0.092	0.888
Delivery method*					0.0:6% | 1.0:65% | 2.0:18% |	0.0:3% | 1.0:45% | 2.0:39% |	2.539	0.845
Neonate sex*					0.0:41% | 1.0:53% |	0.0:32% | 1.0:48% |	0	1
APGAR 1 min*					6.0:6% | 7.0:0% | 8.0:6% | 9.0:82% |	6.0:0% | 7.0:3% | 8.0:7% | 9.0:71% |	2.244	0.845

For continuous variables, if both groups are approximately normal we report mean (SD) [95% CI]; if not normal we report median [Q1–Q3] (P5–P95). Only the appropriate pair (mean-based or median-based) is populated for each feature; the alternative pair is left blank. Categorical variables are shown as percentages in CTRL and GDM. Group comparisons use Welch's *t*-test (normal) or Mann–Whitney *U* (non-normal) for continuous variables, and chi-square for categorical; the corresponding test statistic is reported in "Stat". *p*-values are two-sided; where indicated, multiplicity is controlled with FDR (Benjamini–Hochberg). Statistically relevant differences ($q < 0.05$ or $p < 0.05$ when FDR is not applied) are bolded. Features marked with an asterisk (*) had total non-missing $n < 48$ and should be interpreted with caution. Abbreviations: CTRL, controls; GDM, gestational diabetes mellitus; SD, standard deviation; CI, confidence interval; Q1–Q3, interquartile range; P5–P95, 5th–95th percentiles. Variables marked with * have missing data.

subjects within the WHO-defined categories of normal weight (BMI 18.5–24.9), overweight (BMI 25–29.9), and class I obesity (BMI 30–34.9). Participants were stratified into two groups according to BMI (< 24 and ≥24). Mean BMI was 21.03 ± 1.58 kg/m^2 in the BMI < 24 group and 28.51 ± 3.47 kg/m^2 in the BMI ≥ 24 group. RBC autofluorescence imaging and analysis were performed using the same experimental setup and machine-learning–based segmentation pipeline applied in the main study. Across all cellular compartments, a consistent trend toward higher $AF_{G,R}$ values was observed in subjects with BMI ≥ 24 compared with those with BMI < 24 (Fig. 4). Specifically, $AF_{G,R}$ increased in the core region from −0.13 ± 0.07 to −0.096 ± 0.04, in the membrane region from −0.081 ± 0.07 to −0.032 ± 0.06, and at the whole-cell level from −0.126 ± 0.07 to −0.092 ± 0.04. However, none of these differences reached statistical significance (core: $p = 0.14$; membrane: $p = 0.11$; whole cell: $p = 0.14$). These findings indicate that higher BMI may be associated with mild increases in RBC autofluorescence, although the magnitude and spatial pattern of $AF_{G,R}$ alterations observed in gestational diabetes were not reproduced in this independent non-GDM cohort.

Logistic Regression

A binary logistic regression model was developed to predict group membership (CTRL versus GDM) based on four standardized predictors: BMI, age, MCV, and $AF_{G,R}$ Core. The model was fitted on 43 observations (5 cases were excluded due to incomplete data). It yielded a pseudo-*R*-squared of 0.366 (McFadden), suggesting moderate explanatory power. The model was globally significant, as indicated by the likelihood ratio test ($p = 0.00035$), confirming that the included predictors collectively contribute to the discrimination between the two groups.

As shown in Table 2, BMI emerged as a significant positive predictor ($\beta = 1.87$, $p = 0.007$; OR = 6.47), indicating that higher BMI values are associated with increased odds of belonging to the GDM group. Similarly, $AF_{G,R}$ Core was significantly associated with the outcome ($\beta = 4.93$, $p = 0.018$; OR = 138.6), underscoring its relevance as an independent discriminator of GDM status. In contrast, Age and MCV did not reach statistical significance ($p > 0.8$), indicating limited predictive value within this multivariable model.

Discussion

The present study demonstrates that label-free AF imaging, when combined with machine learning–based segmentation, can detect subtle but significant biophysical alterations in RBCs from women with GDM. By analyzing $AF_{G,R}$ in a compartment-specific manner (core, perimembrane, and whole-cell), we identified a consistent and reproducible shift toward higher $AF_{G,R}$ values in the GDM group compared to healthy controls. These observations open a new perspective on the characterization of gestational diabetes, where membrane dynamics of RBCs have not been thoroughly investigated previously. This shift was evident in all regions examined (Fig. 3, panel E), with greater spatial heterogeneity at the membrane level, although the magnitude of the increase was comparable across compartments. In the core region, GDM RBCs showed a significantly higher mean $AF_{G,R}$ value of −0.073 (±0.202) compared to −0.154 (±0.060) in controls (FDR-adjusted $p = 0.051$). Similarly, in the membrane, GDM samples presented a mean value of 0.013 (±0.198) versus

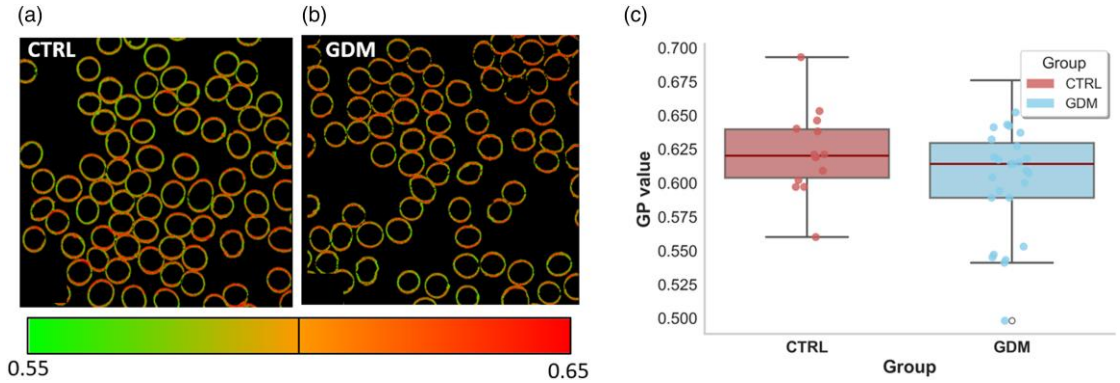

Fig. 2. Membrane fluidity analysis in RBCs from CTRL and GDM groups. (**a, b**) Representative GP maps from RBCs in CTRL and GDM pregnancies, with colormap restricted to 0.55–0.65 to emphasize subtle changes. (**c**) Presents boxplots of GP values across groups. No significant difference in GP values was observed (CTRL: 0.61 ± 0.04 versus GDM: 0.60 ± 0.04, $p = 0.168$), indicating preserved membrane fluidity in GDM, in contrast to alterations typically described in chronic diabetes.

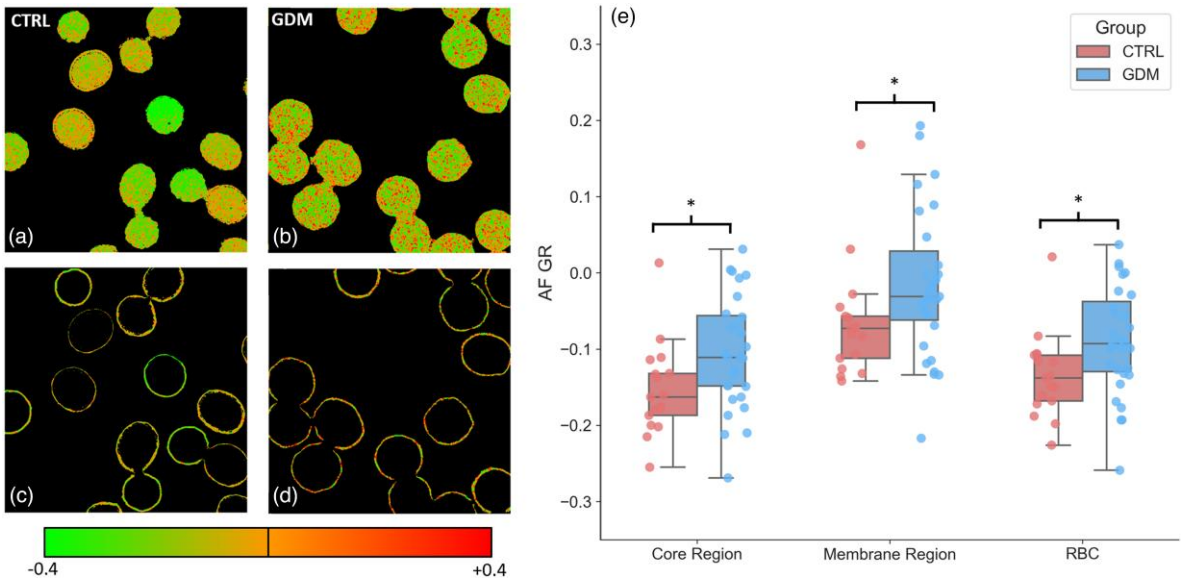

Fig. 3. Compartment-specific autofluorescence ratio between spectral channels (525/50 nm and 595/50 nm) in RBCs from CTRL and GDM groups. (**a,b**) depict core regions and (**c,d**) Perimembrane regions, with colormap set between −0.4 and +0.4. (e) Reports boxplots of autofluorescence ratios in core, membrane, and whole-cell areas. Compared to CTRL, GDM samples showed significantly higher ratios across all compartments (core: -0.073 ± 0.202 versus -0.154 ± 0.060; membrane: 0.013 ± 0.198 versus -0.066 ± 0.075; whole-cell: -0.058 ± 0.199 versus -0.135 ± 0.055; all $p = 0.049$). These results demonstrate increased oxidative/redox imbalance in GDM, captured by autofluorescence mapping, while conventional hematological indices remain unaffected.

−0.066 (±0.075) in the control group ($p = 0.051$). This pattern persisted when evaluating the entire RBC area, where GDM cells showed a value of −0.058 (±0.199) compared to −0.135 (±0.055) in controls ($p = 0.051$). To further investigate the relative contribution of fluorescence-based features compared to conventional clinical variables, we performed a multivariable logistic regression including BMI, age, MCV, and $AF_{G,R}$ Core as predictors. Among these, $AF_{G,R}$ Core remained a statistically significant independent predictor of group membership ($\beta = 4.93$, $p = 0.018$), indicating that its association with GDM status persists after controlling for major confounders. This result highlights the analytical robustness and adds diagnostic value of the $AF_{G,R}$ Core metric. While BMI also emerged as significant, neither age nor MCV contributed meaningfully to the classification, underscoring the specificity of $AF_{G,R}$ Core in capturing relevant signal variation. In clinical terms, the odds ratio associated with $AF_{G,R}$ Core was markedly elevated, supporting its potential as a powerful biomarker. These results suggest that the autofluorescence profile of RBCs is markedly altered in GDM, likely due to a combination of oxidative stress, membrane structural changes, and metabolic remodeling. The increased $AF_{G,R}$ values point toward enhanced green emission, commonly attributed to flavin adenine dinucleotide (FAD), and decreased red emission, associated with porphyrins such as protoporphyrin IX ((Fauaz et al., 2010; Shrirao et al., 2021). This is consistent with previous reports linking diabetes-related oxidative stress to altered RBC redox state and membrane composition (Kolenc & Quinn, 2019; Pitocco et al., 2025). Not only a global increase in $AF_{G,R}$ has been observed in GDM cells but also a distinct spatial heterogeneity, most visible at the perimembrane, where GDM RBCs display irregular and locally intensified fluorescence patterns (Fig. 3). This may reflect early microstructural membrane damage, such as lipid peroxidation

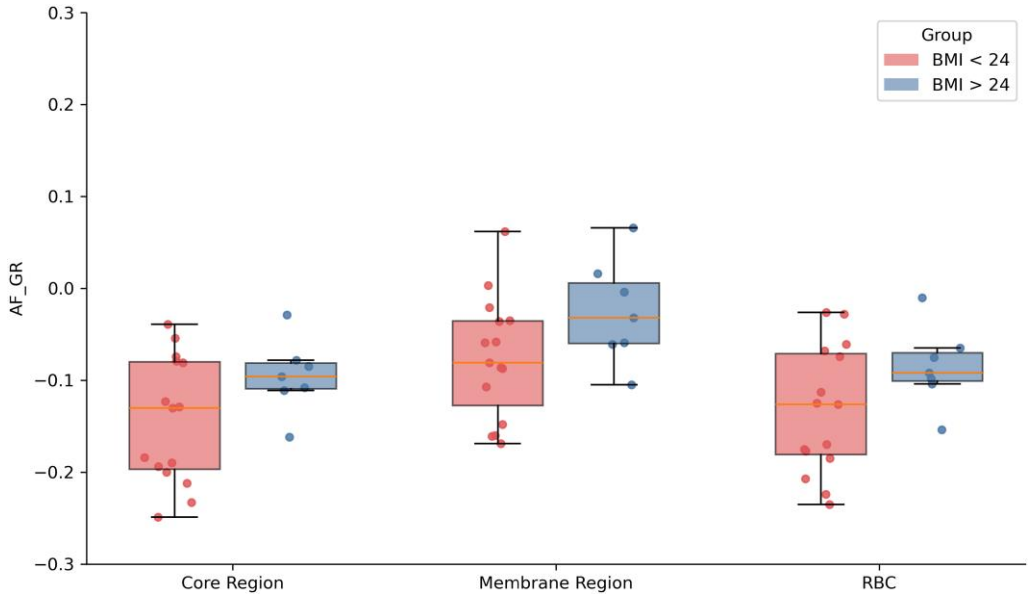

Fig. 4. BMI-associated differences in red blood cell autofluorescence in non-GDM pregnancies. Distribution of the red blood cell autofluorescence ratio ($AF_{G,R}$) between spectral channels (525/50 nm and 595/50 nm) in an independent cohort of pregnant women without gestational diabetes mellitus (non-GDM), stratified by body mass index (BMI < 24; BMI ≥ 24). $AF_{G,R}$ values are reported for the core region, membrane region, and whole-cell (RBC) area. Box plots represent the median and interquartile range, with whiskers indicating the data range and individual points corresponding to single-cell measurements.

Table 2. Logistic Regression Results.

	Coef	Std. err.	z	p Value	IC 95%
const	1.666	0.660	2.526	0.012	0.373–2.959
BMI	1.868	0.694	2.692	**0.007**	**0.508–3.227**
Age	0.093	0.471	0.197	0.844	−0.830–1.016
MCV	0.035	0.445	0.079	0.937	−0.837–0.908
$AF_{G,R}$ *Core*	4.926	2.090	2.356	**0.018**	**0.829–9.023**

Results of the binary logistic regression model predicting the outcome variable *Group* (0 = CTRL. 1 = GDM) based on four standardized covariates. The table reports estimated coefficients (β). standard errors (SE). z-values. p-values and IC 95%. Statistically significant predictors are indicated in bold.

or glycation-induced phase separation, phenomena previously linked to diabetes (Maulucci et al., 2017). Such localized fluidity alterations have also been associated with impaired deformability and increased hemolysis risk in diabetic erythrocytes (Bianchetti et al., 2024).

In contrast, the parallel analysis of membrane fluidity using Laurdan-based GP imaging revealed no significant differences between GDM and control RBCs (CTRL: 0.61 ± 0.04; GDM: 0.60 ± 0.04; $p = 0.168$). This negative result suggests that, unlike in type 1 and type 2 diabetes where significant reductions in GP have been reported (Bianchetti et al., 2021, 2024), GP does not capture measurable alterations in GDM (Fig. 2). This divergence highlights a key point: in chronic diabetes, membrane fluidity is reduced because of long-term lipid remodeling, strongly influenced by diet (e.g., omega-3 uptake) and associated with vascular complications. By contrast, GDM is a transient condition, where the short timescale likely prevents such stable lipid-phase rearrangements. Instead, $AF_{G,R}$ reflects acute oxidative and redox imbalance, emerging as the dominant signature of metabolic stress in pregnancy. Thus, GP and $AF_{G,R}$ should not be seen as redundant but as complementary: the former reports chronic, diet-driven membrane remodeling, while the latter reveals dynamic, redox-related perturbations that characterize gestational diabetes. Notably, although metabolic status and BMI are known to influence oxidative stress in red blood cells, the detection of significant $AF_{G,R}$ alterations in a largely metabolically healthy cohort suggests that this metric is sensitive to mild, pregnancy-specific metabolic stress rather than reflecting chronic adiposity-related alterations alone. Consistently, the BMI-stratified analysis performed in an independent non-GDM cohort (Results, Section 3.4; Fig. 4) showed only mild, non-significant increases in $AF_{G,R}$ with higher BMI, with core values shifting from -0.13 ± 0.07 to -0.096 ± 0.04 ($p = 0.14$), membrane values from -0.081 ± 0.07 to -0.032 ± 0.06 ($p = 0.11$), and whole-cell values from -0.126 ± 0.07 to -0.092 ± 0.04 ($p = 0.14$). Importantly, these BMI-related changes did not reproduce either the magnitude or the spatial autofluorescence pattern observed in gestational diabetes. Together, these findings support the interpretation that $AF_{G,R}$ primarily captures dynamic, pregnancy-related metabolic perturbations associated with GDM rather than baseline metabolic status.

From a clinical standpoint, this means that $AF_{G,R}$ does not replace current diagnostic tests such as the OGTT, which remains the gold standard for GDM detection. Rather, $AF_{G,R}$ provides complementary information on oxidative stress and redox imbalance, dimensions not captured by glucose-based assays. As a non-invasive and repeatable measure, $AF_{G,R}$ could be integrated into clinical workflows to improve risk stratification, identify women at higher risk of complications despite borderline glycemic values, and monitor metabolic stress dynamically during pregnancy and postpartum.

Nevertheless, further experiments will be required to validate this interpretation and disentangle the relative contribution of diet, oxidative stress, and membrane remodeling. These findings are consistent with previous reports of AF alterations in diabetes, where reduced porphyrin-associated red emission (~635 nm) and increased flavin-associated green emission (~525 nm) have been linked to oxidative stress and metabolic dysfunction ((Fauaz et al., 2010, 2010b; Shrirao et al., 2021). Such opposing spectral shifts strengthen the

rationale for using a ratiometric index like $AF_{G,R}$. However, earlier AF studies mostly relied on global spectra or low-resolution imaging, which limited spatial interpretation (Lyons & Basu, 2012; Shrirao et al., 2021). By contrast, our multispectral and compartment-specific approach revealed heterogeneous, membrane-associated alterations that would otherwise remain undetected. From a clinical perspective, $AF_{G,R}$ appears to capture subtle remodeling not reflected in conventional hematological parameters (Table 1). While no differences were observed for Hb, MCV, or WBC, women with GDM showed higher pre-pregnancy BMI ($p = 0.063$), greater glucose excursions during OGTT ($p = 0.003$ at both 60 and 120 min), and slightly shorter gestations ($p = 0.051$). These systemic findings provide a consistent metabolic background to the observed RBC changes. From a translational perspective, the scalability of this approach warrants consideration. The use of a ratiometric autofluorescence metric combined with standardized acquisition parameters enables reproducible comparisons across samples. Because $AF_{G,R}$ is computed pixel-wise and intrinsically normalizes fluctuations in excitation intensity and detector gain, it preserves sensitivity to biologically meaningful spectral redistribution while reducing non-biological variability. Moreover, the imaging and automated analysis workflow relies on widely available microscopy platforms and machine-learning–based segmentation pipelines, supporting potential transferability to larger clinical cohorts. Future integration with higher-throughput optical platforms may further enhance accessibility and clinical applicability. Finally, our label-free strategy offers clear methodological advantages. Unlike Laurdan-based GP imaging, which, although effective, requires exogenous labeling with potential artifacts (Parasassi & Gratton, 1995; Maulucci et al., 2016), AF imaging is entirely non-invasive and records native fluorescence signals, enhancing its translational potential in pregnancy monitoring. However, several limitations must be acknowledged to contextualize these results. First, although the green-to-red autofluorescence ratio provides a sensitive and spatially resolved metric, it remains a composite signal. The spectral overlap of multiple endogenous fluorophores, such as FAD, NAD(P)H, and porphyrins, limits the ability to attribute observed changes to specific biochemical processes. Complementary techniques like fluorescence lifetime imaging (FLIM), hyperspectral unmixing, or targeted metabolomics would be useful to enhance molecular specificity. Second, the cross-sectional nature of our study limits causal interpretation and precludes assessment of longitudinal dynamics. We cannot determine whether the observed AF shifts precede, follow, or parallel the onset of GDM. A longitudinal design would help clarify whether $AF_{G,R}$ could serve as an early predictor or a marker of disease progression. Third, while our sample was carefully curated and demographically consistent, it remains relatively small. Larger and more heterogeneous cohorts, including patients with type 1 or type 2 diabetes, or longitudinal postpartum follow-up, are needed to validate and further confirm these findings.

Conclusion

This study showed that RBC autofluorescence reveals significant alterations in women with gestational diabetes mellitus. By leveraging label-free multispectral imaging and machine learning–based segmentation, we identified consistent increases in $AF_{G,R}$ in the membrane, core, and whole-cell regions of RBCs in GDM. These changes are consistent with redox imbalance and membrane remodeling and suggest that $AF_{G,R}$ mapping may serve as a sensitive, non-invasive biomarker of metabolic stress. Unlike traditional methods requiring exogenous labeling, our approach offers physiological relevance and translational potential. Notably, our data also indicate that GP, a probe of lipid packing and membrane fluidity, does not change in GDM, highlighting the specificity of AF for detecting oxidative and metabolic stress in this condition. However, in chronic diabetes (T1DM and T2DM), where both lipid remodeling and redox imbalance contribute to RBC dysfunction, a combined AF–GP strategy could provide complementary insights into oxidative versus lipid-driven alterations. Future research should explore the longitudinal behavior of $AF_{G,R}$, validate its biochemical underpinnings, and assess its utility as a predictive tool for metabolic complications during pregnancy and maternal and neonatal outcomes.

Availability of Data and Materials

The datasets used and/or analyzed during the current study are available from the corresponding author on reasonable request.

Supplementary Material

To view supplementary material for this article, please visit https://doi.org/10.1093/mam/ozag016.

Acknowledgments

Not applicable.

Consent for Publication

Not applicable.

Author Contributions Statement

A.R. conceptualization, methodology, software, validation, formal analysis, investigation, resources, data curation, writing—original draft preparation, writing—review and editing, visualization. C.N. conceptualization, methodology, software, validation, formal analysis, investigation, resources, data curation, writing—original draft preparation, writing—review and editing, visualization. D.H. methodology, validation, investigation. C.S.: methodology, validation, investigation. M.M.D.G. methodology, validation, investigation. D.A.D. methodology, validation, investigation. D.M. methodology, validation, investigation. A.R. methodology, validation, investigation. L.T. methodology, validation, investigation. L.L.P.: methodology, validation, investigation. M.D.S.: methodology, validation, investigation. G.M. conceptualization, methodology, software, validation, formal analysis, investigation, resources, data curation, writing—original draft preparation, writing—review and editing, visualization, supervision, project administration, funding acquisition. D.P. conceptualization, methodology, validation, investigation, writing—review and editing. All the authors have read and agreed to the published version of the manuscript. All authors have read and agreed to the published version of the manuscript.

Financial Support

This project was supported in part by a research grant awarded to G.M. from Regione Lazio, under the PO FSE 2014-2020 “QUaD2: Una piattaforma e-Health potenziata da algoritmi di machine learning QUantistico per la prevenzione di complicazioni macrovascolari e microvascolari nel

Diabete di tipo 2", co-funded by Blu Sistemi s.r.l, and by a research grant awarded to G.M. by Università Cattolica del Sacro Cuore (Linea D1 2021 programme).

Conflict of Interest

The authors declare that they have no competing interest.

Ethics Standards

This study was conducted in accordance with the Declaration of Helsinki and approved by the Ethics Committee of Università Cattolica del Sacro Cuore (Protocol Code diab_mf). Informed consent was obtained from all the subjects involved in the study. Written informed consent was obtained from the participants to publish this paper.

References

American Diabetes Association Professional Practice Committee. (2024). Introduction and methodology: Standards of care in diabetes—2024. In *Diabetes Care*, **vol. 47**, pp. S1–S4. Arlington, VA: American Diabetes Association Inc, https://doi.org/10.2337/dc24-SINT.

Bianchetti G, Cefalo CMA, Ferreri C, Sansone A, Vitale M, Serantoni C, Abeltino A, Mezza T, Ferraro PM, De Spirito M, Riccardi G, Giaccari A & Maulucci G (2024). Erythrocyte membrane fluidity: A novel biomarker of residual cardiovascular risk in type 2 diabetes. *Eur J Clin Invest* **54**(3), e14121. https://doi.org/10.1111/eci.14121

Bianchetti G, Di Giacinto F, Pitocco D, Rizzi A, Rizzo GE, De Leva F, Flex A, di Stasio E, Ciasca G, De Spirito M & Maulucci G (2019). Red blood cells membrane micropolarity as a novel diagnostic indicator of type 1 and type 2 diabetes. *Anal Chim Acta X* **3**, 100030. https://doi.org/10.1016/j.acax.2019.100030

Bianchetti G, Rizzo GE, Serantoni C, Abeltino A, Rizzi A, Tartaglione L, Caputo S, Flex A, De Spirito M, Pitocco D & Maulucci G (2022). Spatial reorganization of liquid crystalline domains of red blood cells in type 2 diabetic patients with peripheral artery disease. *Int J Mol Sci* **23**(19):11126. https://doi.org/10.3390/ijms231911126

Bianchetti G, Viti L, Scupola A, Di Leo M, Tartaglione L, Flex A, De Spirito M, Pitocco D & Maulucci G (2021). Erythrocyte membrane fluidity as a marker of diabetic retinopathy in type 1 diabetes mellitus. *Eur J Clin Invest* **51**(5):e13455. https://doi.org/10.1111/eci.13455

Chiefari E, Arcidiacono B, Foti D & Brunetti A (2017). Gestational diabetes mellitus: An updated overview. *J Endocrinol Invest* **40**(9), 899–909. https://doi.org/10.1007/s40618-016-0607-5

Croce AC & Bottiroli G (2014). Autofluorescence spectroscopy and imaging: A tool for biomedical research and diagnosis. *Eur J Histochem* **58**(4), 320–337. https://doi.org/10.4081/ejh.2014.2461

Ebenuwa I, Violet PC, Tu H, Lee C, Munyan N, Wang Y, Niyyati M, Patra K, Wilkins KJ, Parrow N & Levine M (2024). Altered RBC deformability in diabetes: Clinical characteristics and RBC pathophysiology. *Cardiovasc Diabetol* **23**(1), 370. https://doi.org/10.1186/s12933-024-02453-2

Fauaz G, Miranda AR, Gomes CZ, Courrol LC, Silva FR, Rocha FG, Schor N & Bellini MH (2010). Erythrocyte protoporphyrin fluorescence as a potential marker of diabetes. *Appl Spectrosc* **64**(4), 391–395. https://doi.org/10.1366/000370210791114248

Kolenc OI & Quinn KP (2019). Evaluating cell metabolism through autofluorescence imaging of NAD(P)H and FAD. *Antioxid Redox Signal* **30**(6), 875–889. https://doi.org/10.1089/ars.2017.7451

Li Y, Liu Y, Liu S, Gao M, Wang W, Chen K, Huang L & Liu Y (2023). Diabetic vascular diseases: Molecular mechanisms and therapeutic strategies. *Signal Transduct Target Ther* **8**(1), 152. https://doi.org/10.1038/s41392-023-01400-z

Lyons TJ & Basu A (2012). Biomarkers in diabetes: Hemoglobin A1c, vascular and tissue markers. *Transl Res* **159**(4), 303–312. https://doi.org/10.1016/j.trsl.2012.01.009

Maulucci G, Cohen O, Daniel B, Sansone A, Petropoulou PI, Filou S, Spyridonidis A, Pani G, De Spirito M, Chatgilialoglu C, Ferreri C, Kypreos KE & Sasson S (2016). Fatty acid-related modulations of membrane fluidity in cells: Detection and implications. *Free Radic Res* **50**, S40–S50. https://doi.org/10.1080/10715762.2016.1231403

Maulucci G, Cordelli E, Rizzi A, De Leva F, Papi M, Ciasca G, Samengo D, Pani G, Pitocco D, Soda P, Ghirlanda G, Iannello G & De Spirito M (2017). Phase separation of the plasma membrane in human red blood cells as a potential tool for diagnosis and progression monitoring of type 1 diabetes mellitus. *PLoS One* **12**(9):e0184109. https://doi.org/10.1371/journal.pone.0184109

McIntyre HD, Catalano P, Zhang C, Desoye G, Mathiesen ER & Damm P (2019). Gestational diabetes mellitus. *Nat Rev Dis Primers* **5**(1), 47. https://doi.org/10.1038/s41572-019-0098-8

Parasassi T & Gratton E (1995). Membrane lipid domains and dynamics as detected by Laurdan fluorescence. *J Fluoresc* **5**(1), 59–69. https://doi.org/10.1007/BF00718783

Pitocco D, Hatem D, Riente A, De Giulio MM, Rizzi A, Abeltino A, Serantoni C, Tartaglione L, Rizzo E, Paoli LL, De Spirito M & Maulucci G (2025). Evaluating red blood cells' membrane fluidity in diabetes: Insights, mechanisms, and future aspects. *Diabetes Metab Res Rev* **41**(1), e70011. https://doi.org/10.1002/dmrr.70011

Rajab AM, Rahman S, Rajab TM & Haider KH (2018). Morphology and chromic Status of red blood cells are significantly influenced by gestational diabetes. *J Hematol* **7**(4), 140–148. https://doi.org/10.14740/jh449w

Saucedo R, Ortega-Camarillo C, Ferreira-Hermosillo A, Díaz-Velázquez MF, Meixueiro-Calderón C & Valencia-Ortega J (2023). Role of oxidative stress and inflammation in gestational diabetes mellitus. *Antioxidants* **12**(10):1812. https://doi.org/10.3390/antiox12101812

Shrirao AB, Schloss RS, Fritz Z, Shrirao MV, Rosen R & Yarmush ML (2021). Autofluorescence of blood and its application in biomedical and clinical research. *Biotechnol Bioeng* **118**(12), 4550–4576. https://doi.org/10.1002/bit.27933